

# Molecular Dynamics of $Q_A^{\cdot-}$ and $Q_B^{\cdot-}$ in Photosynthetic Bacterial Reaction Centers Studied by Pulsed High-Field EPR at 95 GHz

A. Schnegg,<sup>\*,†</sup> M. Fuhs,<sup>†</sup> M. Rohrer,<sup>‡</sup> W. Lubitz,<sup>§</sup> T. F. Prisner,<sup>‡</sup> and K. Möbius<sup>†</sup>

Fachbereich Physik, Freie Universität Berlin, Arnimallee 14, 14195 Berlin, Germany,  
 Institut für Physikalische und Theoretische Chemie, Johann Wolfgang Goethe Universität,  
 Marie Curie Strasse 11, 60439 Frankfurt, Germany, and Max-Planck-Institut für Strahlenchemie,  
 45470 Mülheim an der Ruhr, Germany

Received: February 11, 2002; In Final Form: May 31, 2002

The anisotropic transverse relaxation times  $T_2$  of the primary and secondary acceptor quinone radical anions  $Q_A^{\cdot-}$  and  $Q_B^{\cdot-}$  in Zn-substituted photosynthetic bacterial reaction centers of *Rhodobacter sphaeroides* R26 have been studied by means of 2D high-field/high-frequency (3.4 T/95 GHz, W-band) electron spin-echo spectroscopy. The swept magnetic field is the first, and the pulse-separation time is the second variable. Because of the high magnetic field in W-band EPR, the anisotropic Zeeman interactions of quinone radical anions are resolved; therefore, the orientation dependence of the  $T_2$  relaxation time can be investigated. For  $Q_A^{\cdot-}$  and  $Q_B^{\cdot-}$ , the monoexponential echo decays at 120 K have different orientation-dependent time constants. The anisotropy of the relaxation times is related to anisotropic stochastic fluctuations of the quinones in their protein-binding pockets, which are temperature-dependent. A model is proposed in which the orientation-dependent relaxation originates in reorientational fluctuations around the quinones' specific hydrogen bonds to surrounding amino acids in the binding sites.

## 1. Introduction

Photosynthetic reaction centers (RCs) are pigment-protein complexes in the membranes of green plants and certain bacteria. By coupling electron transfer across the membrane to proton uptake and transmembrane transport processes, RCs convert light energy into chemical energy. In the RC of the purple bacterium *Rhodobacter (Rb.) sphaeroides* R26, the primary electron acceptor,  $Q_A$ , and the secondary electron acceptor,  $Q_B$ , are ubiquinone-10 (UQ-10) molecules.<sup>1,2</sup> Although they are chemically identical,  $Q_A$  and  $Q_B$  show significantly different properties and functions in the light-initiated electron-transfer reaction (i.e.,  $Q_A$  is a one-electron gate that is not protonated and transfers the electron directly to  $Q_B$ ).  $Q_B$ , however, can accept two electrons and two protons before it diffuses out of its binding pocket to be replaced by an unprotonated quinone from the quinone pool.<sup>1,2</sup> For *Rb. sphaeroides*, the X-ray structure is available not only for the dark-adapted EPR silent state<sup>3–6</sup> but also for the light-adapted states  $D^+Q_A^{\cdot-}$ <sup>7</sup> and  $D^+Q_AQ_B^{\cdot-}$  (D stands for the bacteriochlorophyll dimer that is the primary electron donor).<sup>8</sup> From these structures, it was concluded that  $Q_B$  dislocates by as much as 4.5 Å and even performs a 180° propeller twist in its protein pocket when changing from the unreduced to the monoreduced state. Further information about the dark- and light-adapted states in bacterial RCs and the interaction of the cofactors with the protein environment has been obtained by means of vibrational spectroscopy (e.g., FTIR). Generally, the FTIR results are consistent with our findings (see below).<sup>9–11</sup> Quantum mechanical calculations show that in the dark-adapted structure the electron transfer

from  $Q_A$  to  $Q_B$  has a positive reaction energy and is therefore inhibited whereas in the light-adapted structure the reaction energy is negative. This shows that conformational changes control either of the electron-transfer steps from  $Q_A$  to  $Q_B$ .<sup>12–14</sup>

The high-resolution X-ray structure of the binding pockets of the two quinones in the  $D^+Q_AQ_B^{\cdot-}$  state is shown in Figure 1.<sup>8</sup> From a comparison of the X-ray structure with results from EPR and ENDOR experiments, H-bonds of different strengths and symmetries have been deduced between the carbonyl groups of  $Q_A^{\cdot-}$  and  $Q_B^{\cdot-}$  and their protein microenvironment.<sup>1,15,16</sup> For  $Q_A^{\cdot-}$ , a strong H-bond from  $O_4$  to  $N_\delta$  of His(M219) and a weaker one from  $O_1$  to an NH from the peptide backbone of Ala(M260) have been revealed. In the  $Q_B^{\cdot-}$  state, both carbonyl oxygens also form H-bonds with the protein environment. Whereas  $O_4$  is H-bonded to His(L190),  $O_1$  is in contact with three H-bond-forming atoms, the oxygen of Ser(L223), and the backbone nitrogens from Ile(L224) and Gly(L225). Thus, one, two, or even three H-bonds might exist. In addition to the influence of the protein conformation on the electron-transfer characteristics, Okamura et al.<sup>17</sup> showed that fluctuations of the binding pocket, such as vibrational modes of the H-bonds, can also affect the electron-transfer properties. Such a dynamics-structure-function relationship is of great interest in understanding the electron-transfer mechanism in (bacterial) photosynthesis. Molecular motion in solids, glasses, or protein environments may be favorably studied by electron spin-echo (ESE) spectroscopy.<sup>18–20</sup> In particular, for investigating orientation-dependent dynamic line-broadening effects of organic radicals, such as modulations of the resonance frequency through molecular motion, high-field ESE is a very suitable method<sup>21–23</sup> because of its enhanced spectral resolution of small  $g$  tensor anisotropies and its high time resolution.

We have studied the molecular dynamics of  $Q_A^{\cdot-}$  and  $Q_B^{\cdot-}$  by means of 2D high-field/high-frequency ESE at 95 GHz (W-

\* Corresponding author. E-mail: alexander.schnegg@physik.fu-berlin.de.  
 Tel: ++49 30 838-56045. Fax: ++49 30 838-56046.

† Freie Universität Berlin.

‡ Johann Wolfgang Goethe Universität.

§ Max-Planck-Institut für Strahlenchemie.

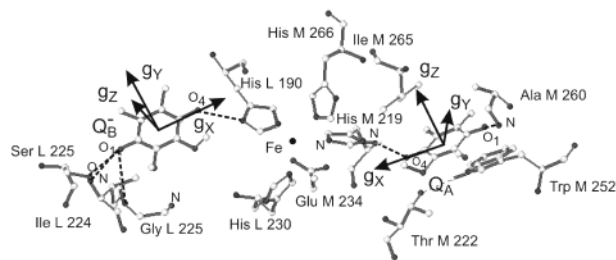


**Figure 1.** Structure of the  $Q_A$  and  $Q_B$  binding sites in the photosynthetic RC of *Rb. sphaeroides* as obtained from the X-ray structure analysis on the charge-separated state,  $D^+Q_B^{\cdot-}$ .<sup>8</sup> For clarity, the isoprenoid chains of the two ubiquinones, UQ-10, are truncated. The angles, which relate the  $g$  tensors of  $Q_A^{\cdot-}$  and  $Q_B^{\cdot-}$  to each other in the state  $Q_A^{\cdot-}Q_B^{\cdot-}$ , are obtained from ref 40. Note that in the present work  $Fe^{2+}$  was replaced by  $Zn^{2+}$ .

band) on RCs of *Rb. sphaeroides* in which  $Fe^{2+}$  was substituted by  $Zn^{2+}$  (Zn-RC). Small-angle fluctuations of the quinones about their equilibrium conformation lead to modulation of the Larmor frequency and, therefore, to enhanced relaxation rates. To quantify these molecular fluctuations, we measured the effective spin-spin relaxation time  $T_2$  by pulsed high-field EPR as the time constant (phase memory time) of the two-pulse echo decay. Because the anisotropy of the  $g$  tensor of  $UQ_{10}^{\cdot-}$  is about  $4 \times 10^{-3}$  and the inhomogeneous line width due to unresolved hyperfine structure is about 1 mT, W-band high-field EPR is required to spread the spectrum over almost 10 mT and to separate the  $X$ ,  $Y$ , and  $Z$  peaks of the  $g$  tensor. Therefore, one can select molecules that are oriented with respect to one of these principal axes along the magnetic field to perform relaxation-rate measurements on these molecules only. Thus, the measurement of the spin-spin relaxation time  $T_{2\text{eff}}$  across the high-field EPR spectrum provides information not only about the correlation time and the amplitude of the small-angle fluctuations but also about the direction of the corresponding axes of such torsional fluctuations in the binding pocket because of the improved orientation selection by the high Zeeman field.

In the  $X$  band, investigations on molecular dynamics by means of ESE-detected EPR was first introduced by Millhauser and Freed<sup>20</sup> and later applied by Dzuba et al.<sup>18</sup> In a previous publication on photosynthetic reaction centers, Rohrer et al.<sup>22</sup> used this method in pulsed W-band high-field EPR to study the stochastic molecular motion of  $Q_A^{\cdot-}$  in *Rb. sphaeroides* and  $UQ_{10}^{\cdot-}$  in 2-propanol solution at 120 K. The dependence of the relaxation rates on the resonance field positions show significant differences for  $UQ_{10}^{\cdot-}$  in the protein environment and in frozen 2-propanol solution. For  $Q_A^{\cdot-}$ , the average of the relaxation times over all resonance positions in the protein environment is about a factor of 2 longer than in frozen 2-propanol. Moreover, whereas in the protein the  $g_X$  resonance position has the longest relaxation time, in 2-propanol,  $T_{2\text{eff}}$  has its maximum at the  $g_Z$  position. Rohrer et al.<sup>22</sup> related the echo-decay functions for each magnetic field position to anisotropic fluctuations of the quinones in their respective binding sites. It was concluded that the quinones undergo reorientational fluctuations around the H-bonds that they form with their local environments. In the present work, we extend this study to  $Q_B^{\cdot-}$  to compare the molecular motion of both ubiquinones in *Rb. sphaeroides* RCs and to learn about dominant H-bonds in the charge-separated states and about the influence of the respective binding pocket on the molecular dynamics of  $Q_A^{\cdot-}$  and  $Q_B^{\cdot-}$ . Furthermore, we have investigated the temperature dependence of the molecular motion of  $Q_A^{\cdot-}$  and of  $Q_B^{\cdot-}$  up to 190 K. This is of particular interest because at higher temperatures charac-

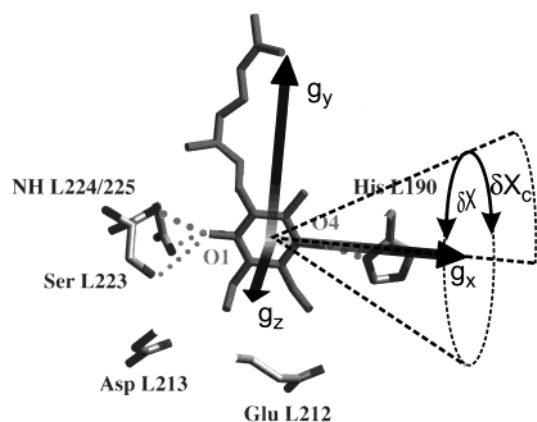


**Figure 2.** Model for the quinone motion on a cone in the RC binding pocket.  $Q_B^{\cdot-}$  and its local protein environment are shown.<sup>8</sup> Possible H-bonds deduced from X-ray and ENDOR studies<sup>1</sup> are indicated by dotted lines. The equilibrium position of the quinone is shown. At 120 K, the dominant H-bond determines the axis about which small-angle fluctuations take place. To a good approximation, this is the  $X$  axis of the quinone  $g$  tensor. These fluctuations are approximated by a two-site jump with rms angle  $\pm\delta X$ . The higher the temperature, the weaker the bonds. As a consequence, at higher temperatures, the libration axis is less precisely fixed in space and may deviate from its equilibrium position. Therefore, we assume that the quinone  $X$  axis is distributed on a cone with an aperture  $\pm\delta X_c$  that increases with increasing temperature.

teristics of the H-bond network are expected to change, as is indicated, for example, by observed changes of the hyperfine structure of  $Q_A^{\cdot-1}$  and possibly of  $Q_B^{\cdot-}$ . This change is most distinct between 100 and 200 K and was attributed to increased H-bond lengths.<sup>1</sup> This should result in decreased bonding strength and, consequently, increased mobility of the radical at higher temperatures. Moreover, it is known that at higher temperatures not only the motion of the cofactor molecule in its binding pocket but also the conformational fluctuations between substates of the protein environment change.<sup>20,24–26</sup>

The quinone cofactor in the RC undergoes molecular motion in a highly structured 3D potential well, which is set up by its binding pocket. In general, this complex motion requires a sophisticated theoretical description, as is given, for example, by Freed and co-workers.<sup>20,24</sup> To simplify the interpretation of the W-band ESE data and to provide a more qualitative model of the temperature-dependent motion of the quinone molecule in its binding pocket, we attempted to refine our previous approach to interpret the pulsed high-field EPR results on  $Q_A^{\cdot-}$  at 120 K.<sup>22</sup> In this model, the overall molecular motion was separated into small-angle fluctuations around the three molecular axes. This is justified as long as the motion is mainly restricted to one of the axes or to very small angles so that the motion can be treated as a linear superposition of torsional oscillations about orthogonal directions. To be able to describe the “weakening” of the H-bonds of the quinone to the binding pocket, we now treat the molecular motion as the motion on a cone with a temperature-dependent aperture around such a weakened H-bond (see Figure 2).

## 2. Theoretical Model

Generally, in the fast-motion limit, the problem of small-angle fluctuations can be treated in the framework of Redfield relaxation theory.<sup>27,28</sup> Assuming that the necessary conditions of fast motion are fulfilled, the Hamiltonian can be split into

the motion-averaged part  $\overline{\mathcal{H}}_0 = \overline{\mathcal{H}}$ , with the bar denoting the time average, and the time-dependent part  $\mathcal{H}'(t)$ :

$$\mathcal{H} = \mathcal{H}_0 + \mathcal{H}'(t) \quad (1)$$

Both parts of the Hamiltonian depend on the equilibrium orientation of the radical with respect to the external magnetic field,  $\mathbf{B}_0$ . This equilibrium orientation, about which the molecule undergoes small-angle fluctuations, will be given by its azimuthal and horizontal polar angles,  $\vartheta$  and  $\varphi$ , respectively, in the principal axes system of the quinone  $g$  tensor (see Figure 1).  $\mathcal{H}_0(\vartheta, \varphi)$  determines the line positions in the EPR spectrum. In the present case, the hyperfine splittings are treated as unresolved contributions to the inhomogeneous line width, thus  $\mathcal{H}_0(\vartheta, \varphi)$  contains only the orientation-dependent Zeeman interaction described by the electronic  $g$  tensor,  $\hat{\mathbf{g}}$ , and  $\mathbf{B}_0$ :

$$\mathcal{H}_0 = \mu_B \hat{\mathbf{S}} \hat{\mathbf{g}} \mathbf{B}_0 \quad (2)$$

Here,  $\mu_B$  is the Bohr magneton, and  $\hat{\mathbf{S}}$  is the vector spin operator of the unpaired electron. This expression is diagonalized by a rotation matrix, which rotates  $\mathbf{B}_0$  from the laboratory frame into the frame of  $\hat{\mathbf{g}}$ .

$$\frac{\mathbf{B}_0^{-1}}{B_0} = \begin{pmatrix} \sin \vartheta \cos \varphi \\ \sin \vartheta \sin \varphi \\ \cos \vartheta \end{pmatrix} \quad (3)$$

Using the effective  $g_{\text{eff}}(\vartheta, \varphi)$  value for a given equilibrium orientation of the molecule with respect to  $\mathbf{B}_0$  and  $m_S$  as the magnetic spin quantum number, the energy eigenvalues are defined:<sup>28</sup>

$$E(\vartheta, \varphi) = \mu_B g_{\text{eff}}(\vartheta, \varphi) B_0 m_S \quad (4)$$

with

$$g_{\text{eff}}(\vartheta, \varphi) = \sqrt{\frac{\mathbf{B}_0^{-1}}{B_0} \cdot \hat{\mathbf{g}} \cdot \hat{\mathbf{g}} \cdot \frac{\mathbf{B}_0}{B_0}} \\ = \sqrt{[g_Z^2 \cos^2 \vartheta + g_X^2 \sin^2 \vartheta \cos^2 \varphi + g_Y^2 \sin^2 \vartheta \sin^2 \varphi]} \quad (5)$$

In the following discussion, we summarize the assumptions made for the interpretation of our ESE experiments and derive an expression for the  $T_2$  relaxation caused by small-angle fluctuations of the quinone in a cone about a dominant H-bond to nearby amino acid:

(1) As outlined above, we assume that it is the  $\hat{\mathbf{g}}$  anisotropy that solely determines the line position of a molecule with a specific orientation with respect to the magnetic field. Therefore, when measuring the echo decay at one particular value of the  $\mathbf{B}_0$  field, one selects molecules with specific  $\vartheta$  and  $\varphi$  angles according to eqs 4 and 5.

(2) The decay time constant of the echo amplitude (i.e., the phase-memory time) is predominantly determined by the spin-spin relaxation time constant  $T_2$ .  $T_2$  may be anisotropic (i.e., dependent on the molecular orientation with respect to  $\mathbf{B}_0$  because of the small-angle fluctuations). However, it is also known that other relaxation processes, such as spin diffusion through spin flips of surrounding protons, exist.<sup>29,30</sup> Nuclear flip-flop transitions ( $\hat{\mathbf{I}}_{1+} \hat{\mathbf{I}}_{2-} - \hat{\mathbf{I}}_{1-} \hat{\mathbf{I}}_{2+}$ ) provide a mechanism for echo dephasing through modulation of the electron-nuclear dipolar coupling. We assume that these other possible mechanisms result in an echo decay that is independent of the molecular orientation with respect to  $\mathbf{B}_0$ , with a time constant  $T_{2\text{iso}}$  (see, for example,

ref 19 and the Discussion). Thus, the transverse relaxation time  $T_{2\text{eff}}$  can be defined as

$$\frac{1}{T_{2\text{eff}}} = \frac{1}{T_2(\vartheta, \varphi)} + \frac{1}{T_{2\text{iso}}} \quad (6)$$

(3) The small-angle fluctuations of the quinone with respect to the laboratory  $\mathbf{B}_0$  field cause fluctuations of the effective  $g$  value. These fluctuations are included in the Hamiltonian (eq 1) as the time-dependent part  $\mathcal{H}'(t)$ . In the Redfield formalism, the relaxation rates are related to the mean-square amplitude of the matrix elements of the perturbation  $\mathcal{H}'(t)$ . For  $T_2$  relaxation, the diagonal matrix elements are the important ones (i.e., we have to calculate the fluctuations in the Larmor frequency). The mean-square amplitude of the  $g$  fluctuation,  $\overline{\delta g^2} = \overline{(g_{\text{eff}} - g(t))^2}$ , is related to the mean-square amplitude of the Larmor frequency fluctuation by

$$\overline{\delta \omega^2} = \frac{\omega_0^2}{g_{\text{eff}}^2} \overline{\delta g^2} \quad (7)$$

Because the Larmor frequency is given by  $\omega_0 = \mu_B g_{\text{eff}} B_0 / \hbar$ , the modulation  $\overline{\delta \omega^2}$  of the Larmor frequency increases quadratically with the external magnetic field and therefore strongly enhances the effects of small-angle fluctuations on the echo decay in high-field EPR. Hence, there is a striking advantage of W-band EPR over X-band EPR for studying such  $g$  tensor-determined dynamics.

(4) Our experiments show that the echo decays are monoexponential. Therefore, the assumption of treating the small-angle fluctuations with correlation time  $\tau_c$  in the fast-motion limit,

$$\overline{\delta \omega^2} \tau_c^2 \ll 1 \quad (8)$$

is justified. The fast-motion assumption is a necessary condition for the validity of Redfield theory.<sup>27</sup> In our case, it is confirmed a posteriori by the results for  $\tau_c$  from the spectra simulations (see below). The measurements also show that the spin-lattice relaxation time  $T_1$  is 2 orders of magnitude longer than  $T_2$  (i.e.,  $T_1 \gg T_2$ ). Therefore, the fluctuation of the Larmor frequency is related to  $T_2$ , according to Redfield theory, by

$$\frac{1}{T_2} = \tau_c \overline{\delta \omega^2} \quad (9)$$

By combining eqs 8 and 9, the validity of the Redfield approximation can be formulated by the condition  $T_2 \gg \tau_c$ , which must be confirmed by the experimental results (see below).

(5) In the preceding article,<sup>22</sup> the  $T_2$  values of  $\text{Q}_A^-$  were measured by field-swept high-field ESE spectroscopy. It was shown that the  $T_2$  values are different for different magnetic field positions in the EPR spectrum. These results have been simulated with a relaxation model in which the quinone undergoes small-angle fluctuations about the three principal axes of the quinone  $g$  tensor that modulate the Larmor frequency. The relaxation rates have been calculated according to eq 9 for fluctuations about the X, Y, and Z axes, respectively, and have been appropriately averaged. It was assumed that the correlation times are equal for all three motions, but that these motions would have different amplitudes ( $\Delta\omega$ ).

Although this model is justified as long as the torsional excursions from equilibrium are small and is successfully used

for low-temperature measurements around 120 K, it lacks physical plausibility when the motion gets more complex, owing to the weakening of the H-bonds at higher temperatures. It was shown that at 120 K the molecular motion of  $Q_A^{\cdot-}$  in its protein binding site takes place most effectively about an axis that is very close to the quinone  $X$  axis (see Figure 1). Therefore, in the present treatment, we assume that the molecule undergoes torsional fluctuations only about this axis, which corresponds to strong H-bonds in this direction. Furthermore, the weakening of the H-bonds at higher temperatures is approximated by allowing this axis to fluctuate as well. Instead of uniaxial fluctuations about the  $X$  axis at low temperatures, at higher temperatures, a model is used in which quinone undergoes fluctuations with amplitude  $\delta X$  on a cone about the  $X$  axis with a fixed but temperature-dependent opening angle  $\delta X_C$  (see Figure 2). Therefore, we calculate the modulation of the Larmor frequency due to a molecular twist with a root-mean-squared (rms) angle-amplitude  $\delta X$  about the momentary  $X$  axis of the quinone  $g$  tensor. The low-temperature orientation of this  $X$  axis is determined by the orientation of the dominant H-bonds of the quinone oxygens with respect to the surrounding protein microenvironment. In our model, the momentary orientation of the  $X$  axis is displaced from its original low-temperature orientation by the angle  $\delta X_C$ . Hence, we have to calculate  $\delta g^2$  by taking into account the twist for all positions on the cone. The matrix that rotates the  $g$  tensor of the quinone to the orientation given by the rms jump angle  $\pm\delta X$  on the cone is

$$\hat{\mathbf{R}}(\pm\delta X, \delta X_C, \alpha) = \hat{\mathbf{R}}_X^{\pm 1}(\delta X) [\hat{\mathbf{R}}_X^{-1}(\alpha) \hat{\mathbf{R}}_Y(\delta X_C) \hat{\mathbf{R}}_X(\alpha)] \quad (10)$$

Here,  $\alpha$  is the angle that denotes the different positions on the cone, about which one has to be averaged to calculate  $\delta g^2$  (see eq 14).

The common rotation matrices<sup>31</sup>

$$\hat{\mathbf{R}}_X(\delta X) = \begin{pmatrix} 1 & 0 & 0 \\ 0 & \cos \delta X & \sin \delta X \\ 0 & -\sin \delta X & \cos \delta X \end{pmatrix} \quad (11)$$

and

$$\hat{\mathbf{R}}_Y(\delta X_C) = \begin{pmatrix} \cos \delta X_C & 0 & \sin \delta X_C \\ 0 & 1 & 0 \\ -\sin \delta X_C & 0 & \cos \delta X_C \end{pmatrix} \quad (12)$$

describe angular transformations about the  $X$  and  $Y$  axes.

Hence, the  $g$  value for the torsional excursions  $\pm\delta X$  is given by

$$g(\vartheta, \varphi, \delta X, \delta X_C, \alpha) =$$

$$\sqrt{\frac{\mathbf{B}_0^{-1}}{B_0} \cdot \hat{\mathbf{R}}(\delta X, \delta X_C, \alpha) \cdot \hat{\mathbf{g}} \cdot \hat{\mathbf{g}} \cdot \hat{\mathbf{R}}^{-1}(\delta X, \delta X_C, \alpha) \cdot \frac{\mathbf{B}_0}{B_0}} \quad (13)$$

Both the excursion about the molecular  $X$  axis and the motion on the cone are part of the stochastic process. The standard deviation of the  $\hat{\mathbf{g}}$  modulation is taken as the amplitude  $\delta g^2$  in eqs 7 and 9 and is given by integration over all possible orientations of the activated molecule:

$$\overline{\delta g^2} = \frac{1}{4\pi} \int_{-\pi}^{\pi} [(g(\vartheta, \varphi, \delta X, \delta X_C, \alpha) - g_{\text{eff}})^2 + (g(\vartheta, \varphi, -\delta X, \delta X_C, \alpha) - g_{\text{eff}})^2] d\alpha \quad (14)$$

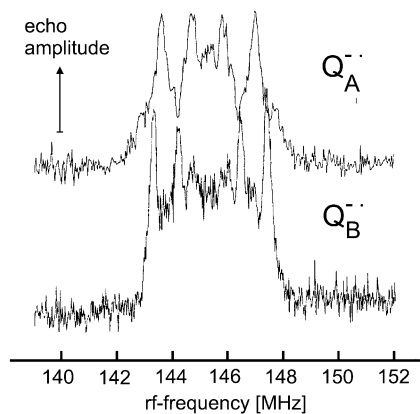


**Figure 3.** W-band Davies ENDOR spectra of  $Q_A^{\cdot-}$  (upper trace)<sup>36</sup> and  $Q_B^{\cdot-}$  (lower trace) at the  $g_z$  position of the EPR spectra ( $T = 160$  K). Independent measurements show<sup>1,33</sup> that the ENDOR spectra of  $Q_A^{\cdot-}$  and  $Q_B^{\cdot-}$  can be distinguished by their hyperfine splittings. No contribution of  $Q_A^{\cdot-}$  to the  $Q_B^{\cdot-}$  spectrum could be detected.

From this expression,  $T_2$  is calculated and then compared with the experimental findings.

### 3. Materials and Methods

To obtain narrow EPR signals from the semiquinone anions,  $Q_A^{\cdot-}$  and  $Q_B^{\cdot-}$ , in bacterial RCs of *Rb. sphaeroides* R26, the high-spin nonheme  $\text{Fe}^{2+}$  ( $S = 2$ ) was replaced by diamagnetic  $\text{Zn}^{2+}$  ( $S = 0$ ) following the procedure of Debus et al.<sup>32</sup> Intact Zn RCs (including the H protein subunit) were obtained after mercury agarose column chromatography (Affigel 501, Biorad). The  $\text{Zn}^{2+}$  content was determined to  $\geq 90\%$  by atomic absorption spectroscopy. The cytochrome *c* photooxidation assay<sup>2</sup> yielded  $1.7 \pm 0.2$  ubiquinone-10 molecules/Zn RC. The Zn RCs were concentrated by ultrafiltration (Amicon centricon 30) to  $\sim 100 \mu\text{M}$  and were transferred into quartz capillaries (0.6 mm i.d., 0.84 mm o.d.) for the W-band experiments. The anion radical  $Q_A^{\cdot-}$  of the primary quinone was generated by continuous illumination of a Zn RC sample for a few seconds with white light near room temperature ( $15^\circ\text{C}$ ) in the presence of a 10-fold excess of cytochrome *c*, followed by rapid freezing in liquid nitrogen. A 1000-W tungsten lamp was equipped with a water filter (8-cm path length) and heat absorbing filter glasses.  $Q_B^{\cdot-}$  was generated in a similar sample by applying a single turnover 3-ns pulse from a Nd/YAG laser ( $50 \text{ mJ/cm}^2$ ). The quinone radicals can be distinguished either by their different  $g_X$  values<sup>1</sup> or by differences in their hyperfine couplings.<sup>33</sup> In the W-band EPR and ENDOR spectra of  $Q_B^{\cdot-}$ , no contribution from  $Q_A^{\cdot-}$  was detected (Figures 3 and 4). This shows that the  $Q_B^{\cdot-}$  sample indeed contained less than a 25% fraction of RCs with  $Q_A^{\cdot-}$  impurities. Care was taken to keep the samples frozen and in the dark during the transfer to the precooled W-band cavity.

The laboratory-built CW and pulsed 95-GHz high-field/high-frequency EPR and ENDOR spectrometer has been described previously.<sup>34,35</sup> The 2D electron spin-echo (2D ESE) spectra were recorded with a  $2/3\pi - \tau - 2/3\pi - \tau$  microwave pulse sequence while stepping the external magnetic field. To measure the echo decay for each magnetic field point, the pulse separation time  $\tau$  was varied. Each data point was averaged 400 times with a repetition rate of 200 Hz. With microwave power of about 12 dBm at the cavity, the  $2/3\pi$  pulse length was between 60 and 120 ns, depending on the quality factor of the loaded cavity.

In the simulations, the spectra of the randomly distributed molecules were obtained by calculating the EPR resonance fields

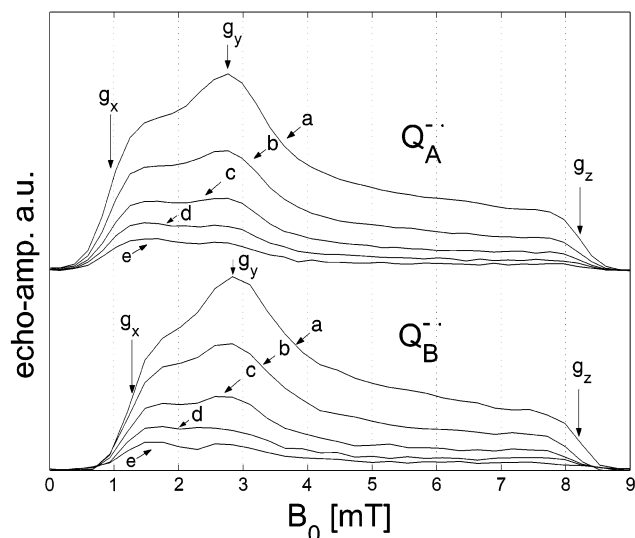


**Figure 4.** W-band ESE-detected EPR spectra of  $Q_A^{\bullet-}$  and  $Q_B^{\bullet-}$  in Zn RCs from *Rb. sphaeroides* at 120 K. The spectra are measured with a  $^{3/2}\pi - \tau - ^{3/2}\pi - \tau$  pulse sequence for different values of  $\tau$ : (a) 100 ns, (b) 300 ns, (c) 500 ns, (d) 700 ns, and (e) 900 ns. The spectra of  $Q_A^{\bullet-}$  and  $Q_B^{\bullet-}$  can be distinguished by their different  $g_x$  values.<sup>41</sup> For longer  $\tau$ , the echo amplitudes decrease and the spectral shape changes because of the orientation dependence of the transverse relaxation time. The spectra are plotted versus  $B_0$  with an offset of 3.34 T.

$B_0$  ( $\vartheta$ ,  $\varphi$ ) for the azimuthal and horizontal angles  $\vartheta$  and  $\varphi$  between 0 and 90° in steps of 0.02°. The hyperfine couplings were taken into account by convolution with a Gauss function with an orientation-independent inhomogeneous line width of 0.6 mT. With the model presented in the previous section, relaxation decays have been calculated for each molecular orientation and added to the 2D spectrum simulation. Fits were obtained using a least-squares fit algorithm when varying  $\delta X$ ,  $\delta X_c$ ,  $\tau_c$ , and  $T_{2\text{iso}}$  (see Discussion). The programs were written using Matlab program language.

#### 4. Results and Discussion

Figure 4 shows the field-swept W-band ESE spectra of  $Q_A^{\bullet-}$  and  $Q_B^{\bullet-}$  at 120 K for different pulse-spacing times  $\tau$  (the spectra recorded with longer  $\tau$  values have smaller amplitudes because of relaxation processes). The arrows in Figure 4 indicate the resonant-field positions that correspond to the principal values of the  $g$  tensor,  $g_x$ ,  $g_y$ ,  $g_z$ , of  $Q_A^{\bullet-}$  and  $Q_B^{\bullet-}$ , respectively. At these field positions, primarily molecules with the orientation of the respective main axis of the  $g$  tensor parallel to  $\mathbf{B}_0$  contribute to the spectrum. The degree of orientational selection is different for the three axes. Only at the  $g_x$  and  $g_z$  positions can single orientations be selected, whereas at the  $g_y$  position, a mixture of different orientations contributes to the EPR signal.<sup>36</sup> The EPR spectra of  $Q_A^{\bullet-}$  and  $Q_B^{\bullet-}$  are distinguished by their different  $g_x$  values, as is seen in Figure 4. Also, the ENDOR spectra differ for  $Q_A^{\bullet-}$  and  $Q_B^{\bullet-}$  when they are recorded at the  $g_x$ ,  $g_y$ , and  $g_z$  field positions (ref 36 and unpublished results). To quantify these observations, the 2D ESE spectra have been fitted with a monoexponential decay function. The dependence of the electron spin-echo amplitude  $S(\tau, B_0)$  on  $\tau$  and  $B_0$  is related to  $T_{2\text{eff}}$  of eq 6 by ref 37:

$$S(2\tau, B_0) = S(0) e^{-2\tau/T_{2\text{eff}}(B_0)} \quad (15)$$

In Figure 5, the fitted  $T_{2\text{eff}}$  values for  $Q_A^{\bullet-}$  and  $Q_B^{\bullet-}$  are presented along the same  $B_0$  axis as the respective ESE spectra at  $\tau = 100$  ns, together with simulations of molecular motion

based on the theoretical model discussed above. As a summary, the following characteristics and differences in the relaxation decays of the ESE spectra of  $Q_A^{\bullet-}$  and  $Q_B^{\bullet-}$  are emphasized. Although the transverse relaxation times of  $Q_A^{\bullet-}$  and  $Q_B^{\bullet-}$  at 120 K are different, they are in the range between  $(1.1 \pm 0.1) \mu\text{s}$  and  $(0.7 \pm 0.1) \mu\text{s}$  for  $Q_A^{\bullet-}$  and  $(1.3 \pm 0.1) \mu\text{s}$  and  $(0.5 \pm 0.1) \mu\text{s}$  for  $Q_B^{\bullet-}$ ; the orientation dependence of the relaxation times is similar.  $T_{2\text{eff}}$  reaches its minimum between the  $g_y$  and  $g_z$  field positions, and the longest relaxation times are found at the  $g_x$  position. At higher temperatures, the differences between  $T_{2\text{eff}}$  at the canonical orientations of  $\hat{\mathbf{g}}$  and at positions between  $g_x$ ,  $g_y$ , and  $g_z$  increase, especially in the well-resolved region between the  $g_y$  and  $g_z$  positions. On the other side, the differences between the relaxation times at the three canonical positions,  $T_{2\text{eff}}^x$ ,  $T_{2\text{eff}}^y$ , and  $T_{2\text{eff}}^z$ , change with temperature. Whereas at 120 K  $T_{2\text{eff}}^x$  is a factor of 2 longer than  $T_{2\text{eff}}^z$  and  $T_{2\text{eff}}^y$ , they become nearly equal at 180 and 190 K. Besides this relative change, an absolute increase of  $T_{2\text{eff}}$  at all spectral positions can be observed between 120 and 160 K. When comparing the relaxation decays of  $Q_A^{\bullet-}$  and  $Q_B^{\bullet-}$ , only few significant differences can be observed; these are discussed below. Using eqs 6–15 of the theoretical model for molecular motion on a cone (section 2), we simulated the 2D ESE spectra for  $Q_A^{\bullet-}$  and  $Q_B^{\bullet-}$  and thereby obtained theoretical  $T_2$  values from the simulated spectra in the same way that we had obtained  $T_2$  values from the experimental spectra. The results are shown in Figure 5. The best-fit results have been obtained with the parameter set given in Table 1. It is admittedly difficult to obtain a unique solution of a problem with so many free parameters. However, it is our experience from additional simulations that the error margins are about 5° for the angle-fluctuation amplitudes, 1 ns for the correlation time  $\tau_c$ , and 0.5  $\mu\text{s}$  for  $T_{2\text{iso}}$ .

At 120 K, the echo decay of  $Q_B^{\bullet-}$  is simulated with a small-angle fluctuation around the molecular  $X$  axis (rms cone aperture  $\delta X_c = 0^\circ$ ) with an rms amplitude  $\delta X = 30^\circ$ . For  $Q_A^{\bullet-}$ ,  $\delta X$  has the same value, but the cone aperture is  $\delta X_c = 7^\circ$ . For both simulations, an isotropic relaxation time of 1  $\mu\text{s}$  had to be included. The reorientational correlation times are 0.3 and 0.5 ns for  $Q_A^{\bullet-}$  and  $Q_B^{\bullet-}$ , respectively.

For higher temperatures, the orientation-dependent relaxation decays of  $Q_A^{\bullet-}$  and  $Q_B^{\bullet-}$  can be simulated satisfactorily only with quite different parameter sets. For  $Q_B^{\bullet-}$ , the rms amplitude of the two-site jump is  $\delta X = 25^\circ$ . The correlation time  $\tau_c = 1$  ns remains constant for all temperatures within the error margins, whereas a distinct increase of  $\delta X_c$  from 3° at 140 K to 25° at 160 K is necessary for a satisfying simulation. To simulate the spectra of  $Q_A^{\bullet-}$ ,  $\delta X$  and  $\tau_c$  have to be drastically changed at 160 and 190 K compared to their values 120 and 140 K. For  $Q_A^{\bullet-}$ , the correlation time increases from 0.5 ns at 140 K to 5.5 ns at 190 K, whereas  $\delta X$  decreases from 24 to 11°.  $\delta X_c$  in  $Q_A^{\bullet-}$  changes from 7 to 14° between 120 and 190 K. The additional isotropic relaxation time  $T_{2\text{iso}}$  increases with higher temperatures for both quinones.

We now discuss possible physical interpretations of the obtained simulation parameters. The successful simulations with the model proposed in section 2 show that at 120 K small-angle fluctuations about the molecular  $X$  axis are the dominating process for transverse spin relaxation. Of course other relaxation effects may exist, for example, those due to time-dependent hyperfine interactions. Fluctuations of the hyperfine couplings can be a result of nuclear spin flips in the vicinity of the quinones<sup>29</sup> or of restricted or unrestricted rotation of substituents (in our case, methoxy or methyl groups). Furthermore, not only the orientation-dependent effective  $g$  value but also the principal

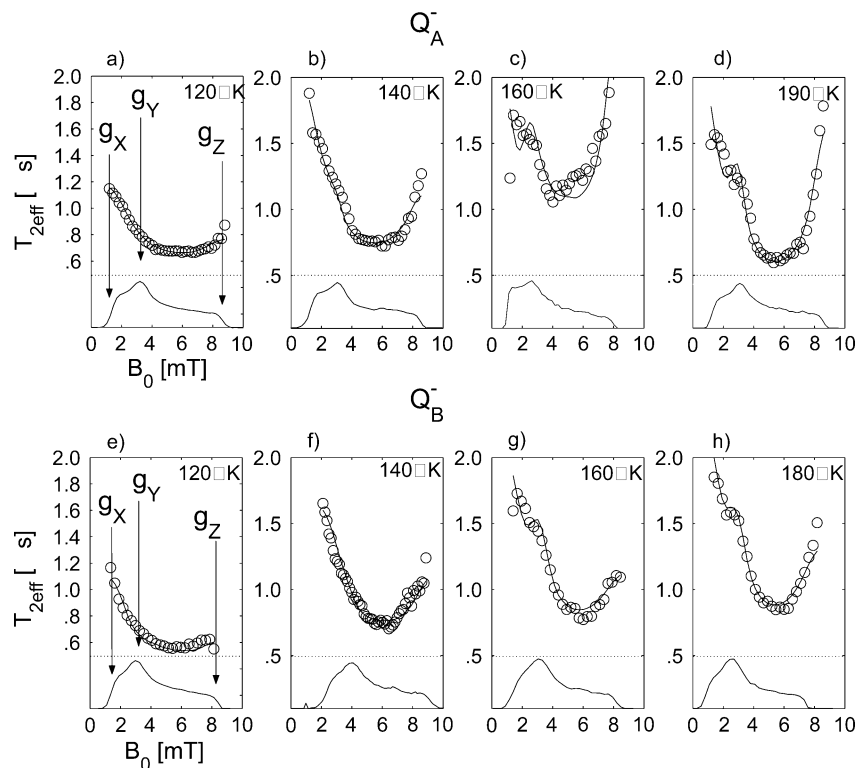


**Figure 5.** Field dependence of  $T_{2\text{eff}}$  for  $Q_A^{-\bullet}$  (a–d) and  $Q_B^{-\bullet}$  (e–h) at 120, 140, 160, and 180 K. In the upper part of the Figure, the transverse relaxation times, as extracted from the echo decays by means of monoexponential functions (eq 15), are represented by circles. The solid lines represent the theoretical  $T_{2\text{eff}}$  values that were obtained from the motional model described in section 2. The obtained fitting parameters are listed in Table 1. In the lower parts of the panels, the field-dependent 2-pulse echo amplitudes (for  $\tau = 100$  ns) are shown as a function of  $B_0$ .

**TABLE 1: Simulation Parameters of the 2D ESE W-Band Spectra of  $Q_A^{-\bullet}$  and  $Q_B^{-\bullet}$**

parameter/ K	$Q_A^{-\bullet}$				$Q_B^{-\bullet}$			
	$\tau_c$ / ns	$\delta X$ / deg	$\delta X_c$ / deg	$T_{2\text{iso}}$ / $\mu\text{s}$	$\tau_c$ / ns	$\delta X$ / deg	$\delta X_c$ / deg	$T_{2\text{iso}}$ / $\mu\text{s}$
120	0.3	30	7	1	0.5	30	0	1
140	0.5	24	12	2	1	20	3	2
160					1	25	25°	5
180					0.5	25	20	5
190	5.5	11	14	3.5				

<sup>a</sup> Parameters have been determined on the basis of the model described in the text (section 2).  $\delta X$  is the rms amplitude of the two-site jump around the  $X$  axis of the quinone  $g$  tensor.  $\delta X_c$  is the aperture of the cone that the libration axis describes (Figure 1), and  $\tau_c$  is the motional correlation time.  $T_{2\text{iso}}$  is an isotropic relaxation-time contribution that is added to the anisotropic  $T_2$  (eq 6). The estimated errors are 1 ns for  $\tau_c$ , 3  $\mu\text{s}$  for  $T_{2\text{iso}}$ , and 5° for the angles. The signal-to-noise ratio for  $Q_A^{-\bullet}$  at 160 K is worse than in the other cases (Figure 5); therefore, no reasonable simulations could be achieved.

values of the  $g$  tensor may be modulated because of structural fluctuations<sup>23</sup> (dynamic  $g$  strain). Modulations of the quinone  $g$  tensor could be a result of changes in H-bond lengths as well as rotation of the methoxy groups. This effect would be mainly observable at the  $g_X$  position. Fluctuations of this component, however, would lead to reduced values of  $T_{2\text{eff}}^X$ . In contrast to this, the experiment shows that  $T_{2\text{eff}}^X > T_{2\text{eff}}^Y, T_{2\text{eff}}^Z$ . Therefore, modulation of principal values of the  $g$  tensor cannot be the dominant source for relaxation in our case. Relaxation resulting from dynamic proton hyperfine interactions could be excluded by measurements on fully deuterated RCs and by 2D ESE at 130 GHz.<sup>38</sup>  $T_2$  measurements on the light-induced radical-pair state  $D^+\cdot Q_A^{-\bullet}$  and on stable  $Q_B^{-\bullet}$  in fully deuterated RCs at 95 GHz (see Figure 6) show the same anisotropies and absolute values for the  $T_2$  relaxation. Therefore,  $T_2$  relaxation in the

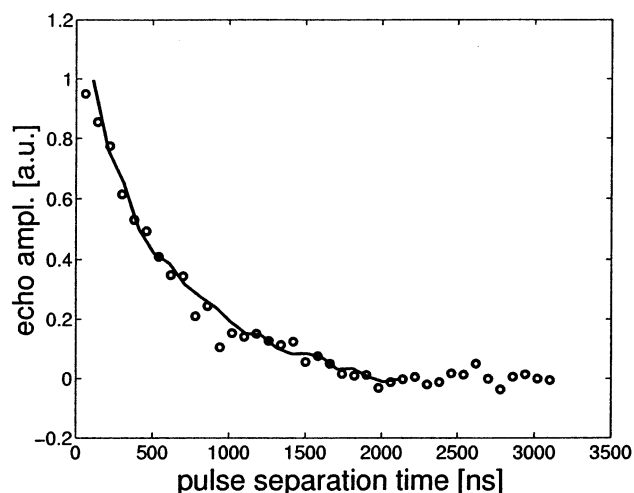


**Figure 6.** Two-pulse echo decay at the  $g_Y$  position of  $Q_B^{-\bullet}$  ( $T = 160$  K) in fully deuterated (O) and wild-type reaction centers (—).

temperature range between 120 and 190 K cannot be influenced by dynamic electron–proton hyperfine interaction, as was suggested by Pashenko et al.<sup>38</sup> Furthermore, EPR measurements on  $Q_A^{-\bullet}$  at 130 GHz between 40 and 120 K<sup>38</sup> have revealed that  $T_2$  relaxation times decrease as compared to those measured at 95 GHz, whereas the relaxation anisotropy at 120 K is similar to that measured at 95 GHz. The observed decrease of the relaxation times at higher magnetic fields  $B_0$  proves in fact that  $T_2$  is induced by the modulation of the  $g$ -tensor orientations (see eq 7). Furthermore, the observation that at 180 K the relaxation times at all principal  $g$  values are nearly the same whereas  $T_2$  values at the positions between the principal  $g$  values are much shorter (see Figure 5) shows that the relaxation

anisotropy is a result of angular excursions of the  $g$  tensor. The related effective  $g$ -value fluctuations have the smallest gradients and, therefore, the smallest effects on  $T_2$  relaxation at the magnetic field positions of the canonical  $g$  tensor values.

Whether stochastic motion of the protein binding pocket, such as transitions between conformational substates,<sup>25,26,39</sup> contributes to the echo decays must still be discussed. If motions of the protein pocket are to contribute to the observed field dependence of  $T_2$  at 120 K, they must be anisotropic with a pronounced  $T_2$  maximum along the  $g_X$  axis of  $Q_A^-$  and  $Q_B^-$ . This, however, is not simultaneously possible for  $Q_B^-$  and  $Q_A^-$  because the  $g_X$  axes of  $Q_A^-$  and  $Q_B^-$  are not parallel.<sup>40</sup> To be responsible for the observed relaxation anisotropy, the protein binding pockets of  $Q_A^-$  and  $Q_B^-$  should fluctuate about axes parallel to  $g_X$  of  $Q_A^-$  and  $g_X$  of  $Q_B^-$  at the same time, which is physically unreasonable. Therefore, we conclude that conformational fluctuations of the quinone binding pocket at 120 K do not contribute to the orientation-dependent  $T_{2\text{eff}}$ . This argument does not hold above 160 K because at higher temperatures the relaxation anisotropy is similar to that of isotropic fluctuations of the  $g$  tensor. Thus, at higher temperatures, it is more difficult to distinguish between relaxation due to isotropic motion or different anisotropic modes of motion. The model presented in this work seems not only to be physically plausible but also to lead to spectra simulations that agree very well with the experimentally observed  $T_2$  anisotropy.

Nevertheless, we want to emphasize that at fixed frequency ESE the echo decay at each molecular orientation contains  $\tau_c \delta\omega^2$  only as a product, and multifrequency ESE would be necessary to separate the product into its factors. Alternatively, we tried to calculate the amplitudes of the fluctuations, calculating  $\delta\omega^2$  from small-angle fluctuations characterized by  $\delta X$ ,  $\delta X_c$ , and keeping these parameters constant for all molecular orientations, our fits and simulations of the spectra showed that it is indeed possible (within the errors given in Table 1) to estimate the correlation time and the amplitude of the fluctuations. The results are summarized in Table 1.

The small-angle fluctuations about the molecular  $X$  axis at 120 K are consistent with the structure of the H-bonds of  $Q_A^-$  and  $Q_B^-$  in their protein pockets as proposed in<sup>1</sup> and shown in Figure 2 for the charge-separated state  $Q_B^-$ . The H-bonds between  $O_4$  and His(L190) and between  $O_1$  and Ser(L225)/Ile(L224) form an axis for the librations that is nearly parallel to the  $g_X$  axis. The orientation dependence of  $T_2$  of  $Q_A^-$  at 120 K can be simulated with nearly the same parameters as those used for  $Q_B^-$ . The main difference is an additional displacement ( $\delta X_c = 7^\circ$ ) of the libration axis of  $Q_A^-$ , which may be due to the less-symmetric binding situation of  $Q_A^-$  as compared to that of  $Q_B^-$ .<sup>1,8</sup>

A possible mechanism for the orientation-independent  $T_{2\text{iso}}$  is spectral diffusion via nuclear spin flips.<sup>29,30</sup> At 120 K,  $T_{2\text{iso}}$  is of the same magnitude as the field-dependent contribution. When the temperature is increased, much longer  $T_{2\text{iso}}$  values are required to simulate the 2D ESE spectra. This behavior is typical for  $T_2$  relaxation as a result of nuclear spin flips. When the temperature of a nonrigid matrix is increased, the rate of motional tumbling increases, which results in longer  $T_{2\text{iso}}$  values.<sup>29</sup>

At 140 K, the values of  $\tau_c$ ,  $\delta X_c$ , and  $T_{2\text{iso}}$  are slightly larger than at 120 K. Increased  $\delta X_c$  and decreased  $\delta X$  values reflect a change in the anisotropy of the small-angle fluctuations. Lubitz and Feher<sup>1</sup> showed that the hydrogen bonds of  $Q_A^-$  become weaker between 80 and 240 K because of thermal expansion of the protein. This may also hold for  $Q_B^-$ , thus providing an

explanation for the increased deviation of the librational axis from the  $X$  direction (i.e., an increase of  $\delta X_c$ ). Although at 140 K the deviation of the quinones'  $g_X$  axes from their equilibrium positions increases, the fluctuations around this  $X$ -axis director are still the relaxation-determining processes.

When  $Q_B^-$  is warmed to 160 K, the spectra-simulation parameters  $\delta X$  and  $\delta X_c$  change significantly. This reflects a change in relaxation anisotropy, which can already be seen from the field dependence of  $T_{2\text{eff}}$  (see Figure 5). Because of the poor signal-to-noise ratio of the 2D ESE spectrum of  $Q_A^-$  at 160 K, no equivalent parameter set could be obtained by simulation. In principle, however, the differences between  $T_{2\text{eff}}^X$ ,  $T_{2\text{eff}}^Y$ , and  $T_{2\text{eff}}^Z$  in  $Q_A^-$  are smaller at 160 K than at 120 and 140 K.

When the temperature is raised from 160 to 180 K, for  $Q_B^-$ , only slight changes can be observed in the orientation dependence of  $T_{2\text{eff}}$  and, correspondingly, in the simulation parameters. For  $Q_A^-$  at 190 K, significantly changed simulation parameters are obtained, as compared to the 120 and 140 K measurements on  $Q_A^-$  and the 180 K measurements on  $Q_B^-$ . As in the case of  $Q_B^-$ , the anisotropy of the small-angle fluctuations changes ( $\delta X \approx \delta X_c$ ). However, for  $Q_A^-$ , the relaxation times at 190 K decrease significantly as compared to those at 160 K. This leads to an unusually large correlation time of 5.5 ns in the spectra simulation according to the relation  $T_2 = (\delta\omega^2 \tau_c)^{-1}$  in the motional-narrowing case.<sup>27,37</sup> The distinct change in relaxation anisotropy between 140 and 160 K may be due to additional fluctuations between conformational substates of the protein that superimpose the fluctuation of the quinone around its H-bond axis. Assuming that these fluctuations are the relaxation-determining process at 180 and 190 K, the experiments show that they affect  $Q_A^-$  and  $Q_B^-$  in different ways. The correlation time obtained from the simulations is a factor of 5 longer for  $Q_A^-$  than for  $Q_B^-$  (see Table 1). This means that the modulations of the  $g$  tensor in  $Q_A^-$  at 190 K are on a much slower time scale than at 120 and 140 K and for  $Q_B^-$ . Slower fluctuations are expected, for instance, for larger subunits of the protein. The assumption of additional conformational fluctuations is in accordance with other spectroscopic data on protein dynamics.<sup>39</sup> By means of Mössbauer spectroscopy,<sup>25,26</sup> it was shown that in bacterial RCs between 150 and 200 K a dynamic conformational transition takes place in the protein microenvironments of  $Q_A$  and  $Q_B$ . At temperatures below 150 K, protein motion is dominated by solid-state vibrations; however, at higher temperatures, fluctuations between conformational substates of the rough energy surface of the protein dramatically increase.

In the temperature regime above 150 K, the parameters obtained from the ESE simulations have to be interpreted with care. It should be pointed out that the relaxation decays are still monoexponential and, therefore, the fluctuations ought to be fast compared to the pulse-separation time. Although different conformational fluctuations may result in orientation-dependent relaxation decays similar to those of isotropic motion with only one correlation time, they probably are anisotropic and occur over a broad range of time scales. For such complex modes of motion, the quantities obtained on the basis of the model proposed in this work may no longer describe the motion in physical detail. Nevertheless, our method is sensitive to the temperature dependence of cofactor motions and conformational fluctuations in the protein. This is of particular interest because it was recently shown<sup>26</sup> that this temperature-dependent change in protein conformation coincides with a blocking of the electron transfer from  $Q_A^-$  to  $Q_B$ . This holds for bacterial RCs and for

PSII in plant photosynthesis. It was concluded that the formation of  $Q_B^{\bullet-}$  occurs only in a highly flexible protein environment.

## 5. Conclusions

In a high-field (W-band) 2D ESE study, the temperature dependence of the transverse relaxation times of the acceptor radical anions  $Q_A^{\bullet-}$  and  $Q_B^{\bullet-}$  in Zn-substituted photosynthetic reaction centers of *Rb. sphaeroides* has been investigated. Because of the high spectral resolution of W-band EPR, well-resolved powder patterns resulting from the orthorhombic  $g$  tensor of the quinone anions could be recorded. As a result of the quadratic field dependence of the transverse relaxation rate,  $T_2^{-1} = \tau_c \cdot \delta\omega^2 = \tau_c \cdot (\mu_B/\hbar)^2 \cdot \delta g^2 \cdot B_0^2$ , echo-decay studies of molecular motion in the W band are 100 times more sensitive to modulations of the effective  $g$  value than are similar measurements at X-band frequencies.

The 2D ESE spectra can be successfully simulated using a theoretical model of molecular motion in which small-angle fluctuations of the quinones about their  $g$  tensor axes are considered to be the dominant  $T_2$  relaxation mechanism. These fluctuations take place with rather short correlation times (around 1 ns) in the binding pocket of the quinones made up by the protein microenvironment. To describe the change of the fluctuation anisotropy with increasing temperature, we allowed the fluctuation axis to deviate within a cone about its equilibrium orientation. The simulations show that this model is adequate for the torsional motions observed at 120 and 140 K. At higher temperatures, however, the cone aperture is of the same magnitude as the fluctuation jump angle. This may reflect the fact that the motion becomes more and more isotropic at these temperatures and that the model becomes inadequate to describe the situation.

When comparing the results for  $Q_A^{\bullet-}$  and  $Q_B^{\bullet-}$ , the main characteristics are very similar; however, they differ in the details. Both quinones show anisotropic fluctuations at 120 and 140 K, and for both molecules, the fluctuation axes lie along their dominant H-bond directions to amino acids of the protein pocket. The different symmetry of the H-bonds of  $Q_A^{\bullet-}$ , compared to that of  $Q_B^{\bullet-}$ , is reflected in larger deviations of the fluctuation axis from its orientation at 120 K. Additionally, for the simulations at 190 K, a very long  $\tau_c$  is needed for  $Q_A^{\bullet-}$ , as compared to that of  $Q_B^{\bullet-}$  at 180 K. Hence, low-temperature measurements of the relaxation times at different resonance positions reveal important structural details such as H-bond directions. At temperatures higher than 160 K, the motional modes lose their directional preference. Such changes of motional anisotropy are of great interest because they may be closely connected to conformational fluctuations of the protein that are mandatory for the electron transfer from  $Q_A^{\bullet-}$  to  $Q_B$  in photosynthesis. A principal restriction of  $T_2$  measurements at only one microwave frequency is that the rms amplitude  $\delta\omega$  and the correlation time  $\tau_c$  of molecular motions cannot be separated but are determined as a product. However, as discussed previously, theoretical estimates can be made on the basis of a simple model of gyroscopic motion. Additional evidence for our values for correlation times and amplitudes of the fluctuations as well as for the relaxation mechanisms that our analysis is based on is expected from future high-field EPR experiments at 180 and 360 GHz. Such experiments are planned for the near future. They should elucidate the temperature dependence of the different relaxation mechanisms and correlation times and should provide information with respect to motion and structure that is important for a better understanding of the structure–dynamic–function relationship. In addition,

high-field EPR experiments are planned on quinone anions in solvents with different polarities and hydrogen-bonding capabilities to modulate the binding network of the quinones. Applications of the experimental methods presented in this work to quinone radicals in other protein complexes are in progress.

**Acknowledgment.** Stimulating discussions with Martin Plato (FU Berlin), Jack Freed and Keith Earle (Cornell University, Ithaca, NY), and Evgeniya Kirilina (Novosibirsk State University, Russia) are gratefully acknowledged. We are grateful to Ed Abresch (University of California—San Diego, San Diego, CA) for his advice concerning the preparation of the Zn RCs from *Rb. sphaeroides*. This work was supported by the Deutsche Forschungsgemeinschaft (SFB 498 and SPP 1051).

## References and Notes

- (1) Lubitz, W.; Feher, G. *Appl. Magn. Reson.* **1999**, *17*, 2.
- (2) Okamura, M. Y.; Debus, R. J.; Kleinfeld, D.; Feher, G. Academic Press: New York 1982; pp 299–317.
- (3) Allen, J.; Feher, G.; Yeats, T.; Rees, D.; Deisenhofer, J.; Michel, H.; Huber, R. *Proc. Natl. Acad. Sci. U.S.A.* **1986**, *83*, 8589.
- (4) Allen, J.; Feher, G.; Yeats, T.; Komiya, H.; Rees, D. *Proc. Natl. Acad. Sci. U.S.A.* **1987**, *84*, 5730.
- (5) Allen, J.; Feher, G.; Yeats, T.; Komiya, H.; Rees, D. *Proc. Natl. Acad. Sci. U.S.A.* **1987**, *84*, 6162.
- (6) Allen, J.; Feher, G.; Yeats, T.; Komiya, H.; Rees, D. *Proc. Natl. Acad. Sci. U.S.A.* **1987**, *84*, 6438.
- (7) Abresch, E. C.; Yeh, A. P.; Soltis, S. M.; Rees, D. C.; Axelrod, H. L.; Feher, G. *Biophys. J.* **1999**, *76*, A141.
- (8) Stowell, M. H.; McPhillips, T.; Rees, D. C.; Soltis, S. M.; Abresch, E. C.; Feher, G. *Science (Washington, D.C.)* **1997**, *276*, 812.
- (9) Breton, J.; Boullais, C.; Berger, G.; Mioskowski, C.; Nabedryk, E. *Biochemistry* **1995**, *34*, 11606.
- (10) Buchanan, S.; Michel, H.; Gerwert, K. *Biochemistry* **1992**, *31*, 1314.
- (11) Budler, R.; de Groot, H.; van Liemt, W.; Steggerda, W.; Esmeijer, R.; Gast, P. *EMBO J.* **1994**, *13*, 5523.
- (12) Kleinfeld, D.; Okamura, M. Y.; Feher, G. *Biochemistry* **1984**, *23*, 5780.
- (13) McMahon, B.; Müller, J. D.; Wraight, C. A.; Nienhaus, G. U. **1998**, *74*, 2567.
- (14) Rabenstein, B.; Ullmann, G.; Knapp, E. W. *Biochemistry* **2000**, *39*, 10487.
- (15) Lubitz, W.; Abresch, E. C.; Debus, R. J.; Isaacson, R. A.; Okamura, M. Y.; Feher, G. *Biochim. Biophys. Acta* **1985**, *808*, 464–469.
- (16) Feher, G.; Isaacson, R. A.; Okamura, M. Y.; Lubitz, W. In *Antennas and Reaction Centers of Photosynthetic Bacteria: Structure, Interactions, and Dynamics*; Beyerle, M. E. M., Ed.; Springer Series in Chemical Physics; Springer-Verlag: Berlin, 1985; pp 174–189.
- (17) Feher, G.; Okamura, M.; Kleinfeld, D. In *Protein Structure: Molecular and Electronic Reactivity*; Austin, R., Buhks, E., Chance, B., DeVault, D., Dutton, P. L., Frauenfelder, H., Goldanskii, V. I., Eds.; Proceedings in Life Sciences; Springer-Verlag: New York, 1987; pp 339–421.
- (18) Dzuba, S. A.; Tsvetkov, Y. D.; Maryasov, A. G. *Chem. Phys. Lett.* **1992**, *188*, 217.
- (19) Dzuba, S. A. *Spectrochim. Acta, Part A* **2000**, *56*, 227.
- (20) Millhauser, G. L.; Freed, J. H. *J. Chem. Phys.* **1984**, *81*, 37.
- (21) Prisner, T. *Adv. Opt. Magn. Reson.* **1997**, *20*, 245.
- (22) Rohrer, M.; Gast, P.; Möbius, K.; Prisner, T. *Chem. Phys. Lett.* **1996**, *259*, 523.
- (23) Poluektov, O.; Doubinski, A. *Chem. Phys. Lett.* **1998**, *288*, 841.
- (24) Saxena, S.; Freed, J. H. *J. Phys. Chem.* **1997**, *101*, 7998.
- (25) Parak, F.; Frolov, E. N.; Kononenko, A. A.; Mössbauer, R. L.; Goldanskii, V.; Rubín, A. *FEBS Lett.* **1980**, *117*, 368.
- (26) Garbers, A.; Reifarh, F.; Kurreck, J.; Renger, G.; Parak, F. *Biochemistry* **1998**, *37*, 11399.
- (27) Redfield, A. G. *Adv. Magn. Reson.* **1965**, *1*, 1–32.
- (28) Atherton, N. M. *Principles of Electron Spin Resonance*; Ellis Horwood Ltd.: Chichester, England, 1993.
- (29) Brown, I. M. In *Time Domain Electron Spin Resonance*; Kevan, L., Schwartz, R. N., Eds.; Wiley and Sons: New York, 1979; pp 195–231.
- (30) Zecevic, A.; Eaton, G. R.; Eaton, S. S.; Lindgren, M. *Mol. Phys.* **1998**, *95*, 1255.
- (31) Goldstein, H. *Classical Mechanics*, 2nd ed.; Addison-Wesley Press, Inc.: Cambridge, MS., 1980; p 109.
- (32) Debus, R. J.; Feher, G.; Okamura, M. *Biochemistry* **1986**, *25*, 2276.

- (33) Isaacson, R. A.; Abresch, E. C.; Paddock, M.; Feher, G.; Lenzian, F.; Lubitz, W. *Biophys. J.* **1998**, A135.
- (34) Burghaus, O.; Rohrer, M.; Götzinger, T.; Plato, M.; Möbius, K. *Meas. Sci. Technol.* **1992**, 3, 765.
- (35) Prisner, T.; Rohrer, M.; Möbius, K. *Appl. Magn. Reson.* **1994**, 7, 167.
- (36) Rohrer, M.; MacMillan, F.; Prisner, T. F.; Gardiner, A.; Möbius, K.; Lubitz, W. *J. Phys. Chem. B* **1998**, 102, 4648.
- (37) Thomann, H.; Dalton, L. R.; Dalton, L. A. In *Biological Magnetic Resonance*; Berliner, L. J., Ed.; Plenum Press: New York, 1990; Vol. 6.
- (38) Pashenko, S.; Gast, P.; Hoff, A. In *Proceedings of the 12th International Congress on Photosynthesis*, Brisbane, Australia, 2001; p 83.
- (39) Steinhoff, H. J.; Karim, C. *Ber. Bunsen-Ges. Phys. Chem.* **1993**, 97, 163.
- (40) Calvo, R.; Abresch, E. C.; Bittl, R.; Feher, G.; Hofbauer, W.; Isaacson, R. A.; Lubitz, W.; Okamura, M. Y.; Paddock, M. L. *J. Am. Chem. Soc.* **2000**, 122, 7327.
- (41) Isaacson, R. A.; Lenzian, F.; Abresch, E. C.; Lubitz, W.; Feher, G. *Biophys. J.* **1995**, 69, 311.